Vietnam Journal of Earth Sciences, 1-26, https://doi.org/10.15625/2615-9783/16864

Vietnam Academy of Science and Technology
Vietnam Journal of Earth Sciences
http://www.vjs.ac.vn/index.php/jse

Recharge mechanism and salinization processes in coastal aquifers in Nam Dinh Province, Vietnam

Hoang Van Hoan[1], Flemming Larsen[2], Pham Quy Nhan[3*], Tran Vu Long[4], Nguyen Thi Thanh Giang[5]

[1]*National Center for Water Resources Planning and Investigation, Hanoi, Viet Nam*
[2]*Geological Survey of Denmark and Greenland, 10, Øster Voldgade, DK-1350 Copenhagen K, Denmark*
[3]*Hanoi University of Natural Resources & Environment, Hanoi, Viet Nam*
[4]*Hanoi University of Mining and Geology, Hanoi, Viet Nam*
[5]*University of Transport and Communications, Hanoi, Viet Nam*

Received 05 September 2021; Received in revised form 27 November 2021; Accepted 27 December 2021

ABSTRACT

In Nam Dinh province, in the Red River delta plain in Northern Vietnam, groundwater in the shallow Holocene aquifer shows elevated total dissolved solids up to 35 km from the coastline, indicating a saltwater intrusion from the Gulf of Tonkin. High groundwater salinities have been encountered below and adjacent to the Red River in the deep Pleistocene aquifer. Since 1996, large-scale groundwater abstraction was initiated from the deep aquifer, and the observed elevated salinities now raise concerns about whether the groundwater abstraction is undertaken sustainably. We have conducted a study to obtain a fundamental understanding of the recharge mechanisms and salinization processes in the Nam Dinh province. A holistic approach with multiple methods including transient electromagnetic sounding and borehole logging, exploratory drilling, sampling and analyzing major ions and stable isotope compositions of water and pore water, groundwater head monitoring, hydraulic experiments laboratory of clay layers, and groundwater modeling by using the SEAWAT code. Results reveal that saline river water is leached from the Red River and its distributaries into the shallow aquifers. The distribution and occurrence of salty pore water in the Holocene aquitard clay shows that meteoric water has not been flowing through these low permeable clay layers. Marine pore water has, however, been leached out of the Pleistocene clay. When this layer is present, it offers protection of the lower aquifer against high salinity water from above. Salinity as high as 80 % of oceanic water is observed in interstitial pore water of the transgressive Holocene clay. Saltwater is transported into the Pleistocene aquifer, where the Holocene clay is directly overlying the aquifer.

Keywords: Holocene transgression, recharge mechanism, salinization processes, interstitial salty pore water, geophysical survey, SEAWAT modeling, Vietnam.

1. Introduction

Nam Dinh province is located in the Red River delta plain of Vietnam (RRDP), where large-scale domestic and commercial groundwater abstraction was initiated in 1994 from the Pleistocene aquifer in alluvial deposits. This groundwater abstraction of about 218,000 cubic meters per day has initiated a drawdown in the Pleistocene

*Corresponding author, Email: pqnhan@hunre.edu.vn

aquifer of up to 9 meters, and the sustainability of the water abstraction has therefore been questioned. Groundwater total dissolved solids (TDS) in the Pleistocene aquifer is highest in the northeastern part of the province, adjacent to the Red River, with values up to 6 g/L (Fig. 1). In the shallow Holocene aquifer, elevated groundwater TDS have been observed in the RRDP at distances up to 35 km from the Gulf of Tonkin (Tran et al., 2012), and high groundwater salinity has also been observed in a shallow aquifer in the Nam Dinh province (Hoang et al., 2011).

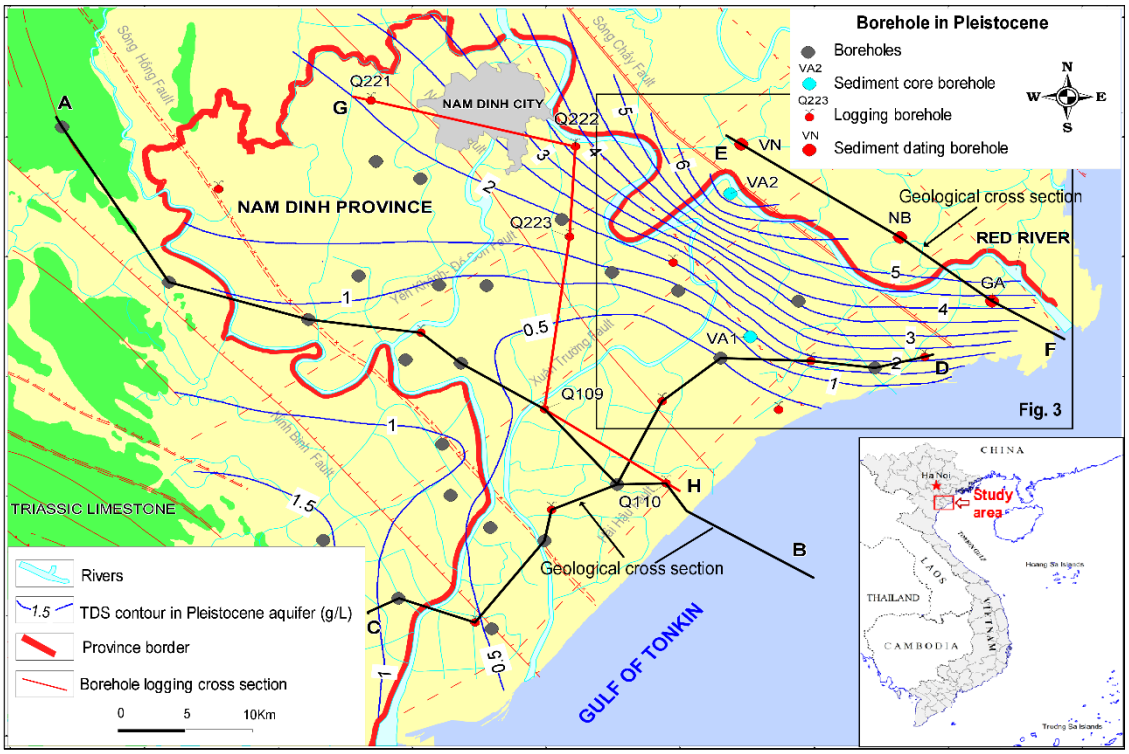

Figure 1. Map showing the location of the Nam Dinh province in the Red River delta plain, and the distribution of total dissolved solids in the Pleistocene aquifer. The locations of the geological cross-sections depicted in Fig. 2 are also shown

The source of the groundwater salinity in the aquifers in the Nam Dinh province is still debated, as both saltwater intrusions through the sea bed and from the many tributaries of the Red River can take place (Vu 1996; Pham, 2004). Alternatively, the elevated groundwater TDS source could be the leakage of paleo-saltwater from transgressive Holocene marine clays, a process which has been documented to occur in the province (Tanabe et al., 2006; Tran et al., 2012). Paleo-water has been defined as groundwater that originated in colder climatic conditions of the Late Pleistocene (e.g., Edmunds, 2001). Still, the term refers to marine pore water entrapped in low permeable sediments (Larsen et al., 2017). In near coastal sediments, trapped marine pore water might be diluted with fresh water flowing from rivers in the delta, and therefore not necessarily have an initial oceanic saltwater composition with 20,000 mg/L chlorides.

Several authors have reported elevated groundwater salinities adjacent to rivers in coastal zones, and this has been ascribed to saltwater intrusions into the rivers and

subsequent leaching to the adjacent shallow aquifers (e.g., Neilson-Welch and Smith 2001; Kolker et al., 2013). In the Gulf of Tonkin delta systems, where typhoons frequently occur from May to November, saltwater intrusions have been studied in the Mekong delta by Nguyen et al. (2008), in the Pearl River delta by Zhang et al. (2013), and in the Red River by Vu (1996) and Pham (2004). The latter studied salinity intrusions in nine rivers in the Red River estuary, using satellite multispectral images and tidal tables covering 1960 to 1982. The result reveals that during the monsoon seasons, with a high freshwater discharge from the rivers, the salinity in the estuary is low with values between 9 and $17^{o}/_{oo}$, whereas in the dry season's salinity increased to 23 and $32^{o}/_{oo}$ as far inland as 35 to 40 km. Vu (1996) also reported salty water in the Red River as far inland as 35 km from the coastline.

In short, saltwater occurrence in the RRDP in Holocene and Pleistocene aquifers has previously been described on a regional scale (Pham, 2000; Nguyen, 2005; Tran et al., 2012), and in the Nam Dinh province (Nguyen 2009; Wagner et al., 2011). Salty groundwater originating from this trapped seawater is still present in Holocene-aged sediments with low permeability in the Red River delta. It affects groundwater salinity in adjacent aquifers while trapped seawater from all Pleistocene-aged sediments leached (Larsen et al., 2017). Hoan et al. (2020) have focused on the Southern part of the Red River delta and raised a conceptual model for salt groundwater intrusion in the Pleistocene aquifer by vertical saltwater leakage from upper Holocene marine sediments that were controlled by the diffusion and density flow and horizontal saltwater intrusion due to high hydraulic gradient generated with over groundwater exploitation. To set up proper management of the groundwater resources in the coastal regions still requires an improved conceptual understanding regarding recharge mechanisms, and the source of the salinity in the aquifers needs to be clarified. Therefore, the overall aims of this study are to obtain such a fundamental understanding; more specifically, to elucidate the recharge mechanism by which freshwater is replenishing abstracted groundwater in the study area and gain an understanding of the processes controlling salinity of the abstracted water.

2. Sea-level history and geological setting of Nam Dinh province

An understanding of the sources of salinities in the Nam Dinh province, and especially the occurrence of paleo-saltwater, cannot be obtained without an insight into the geological development during the Quaternary period. Based on studies of cored sediments, the near-surface geology has been characterized as formed in a wave-dominated delta front with a landscape consisting of alternating beach and inter-ridge marshes (Hori et al., 2004; Tanabe et al., 2006; Funabiki et al., 2007). The eustatic sea-level changes in the Gulf of Tonkin controlled deposits forming in the RRDP during the Quaternary period, hereafter just sea level. The development in sea level during the last 200,000 years (200 ka). During the latest part of the Middle Pleistocene period, from 200 to 130 ka, the sea level was low during a glaciation, and coarse-grained deposits were deposited in the RRDP. The sea level was relatively high, around 130 ka, during the previously interglacial period (Eemian). Still, after then, in the Late Pleistocene, between 130 and 20 ka, the sea level again gradually declined to a low level of around 130 meters below the present sea level (mbsl). With race sea level, the valleys were filled with marine sediments during this period. From 6 ka, the sea level increased to its present status and was even 3 to 4 meters above the current sea level (masl) between 6 and 4 ka (Tanabe et al., 2006). During this Late Holocene maximum sea-level stand, a transgression was

initiated, and shallow terraces with marine sediments were deposited. From 4 ka, the sea level declined and reached its present level in the Gulf of Tonkin, and this fall initiated the recent a progradation of the Red River delta front (Tran et al., 1991; Tanabe et al., 2006).

The near subsurface geology in the Nam Dinh province is compiled in three cross-sections in Fig. 2. Triassic limestone is outcropping west of the Nam Dinh province, and Neogene silty sandstones underlie the Quaternary deposits in the central parts of the province (Fig. 2a, b). Middle and Late Pleistocene coarse-grained alluvial and fluvial deposits are overlying the Triassic and Neogene deposits, and these layers are encountered at depths from ~ 70 m to ~130 m below the surface (mbs). Late Pleistocene marine clay, probably from an Eemian transgression, overlooks Early Holocene transgressive marine clays (Fig. 2). The interlaying sandy deposits between these clays must be interpreted as representing remains of fluvial systems from paleo-rivers in the delta plain. The transgressive, Holocene marine clay is in the Nam Dinh province, encountered at depth from ~ 10 and to ~ 60 mbs, and C-14 dating of these sediments reveals a deposition from 10 to 1 ka (Tanabe et al., 2006). The sediment ages decrease upward and towards the coast (Fig. 2c). The uppermost ~10 m of the subsurface consists of Late Holocene to recent delta plain and delta front deposits composed of organic-rich sandy, silty, and clayish deposits (Fig. 2c).

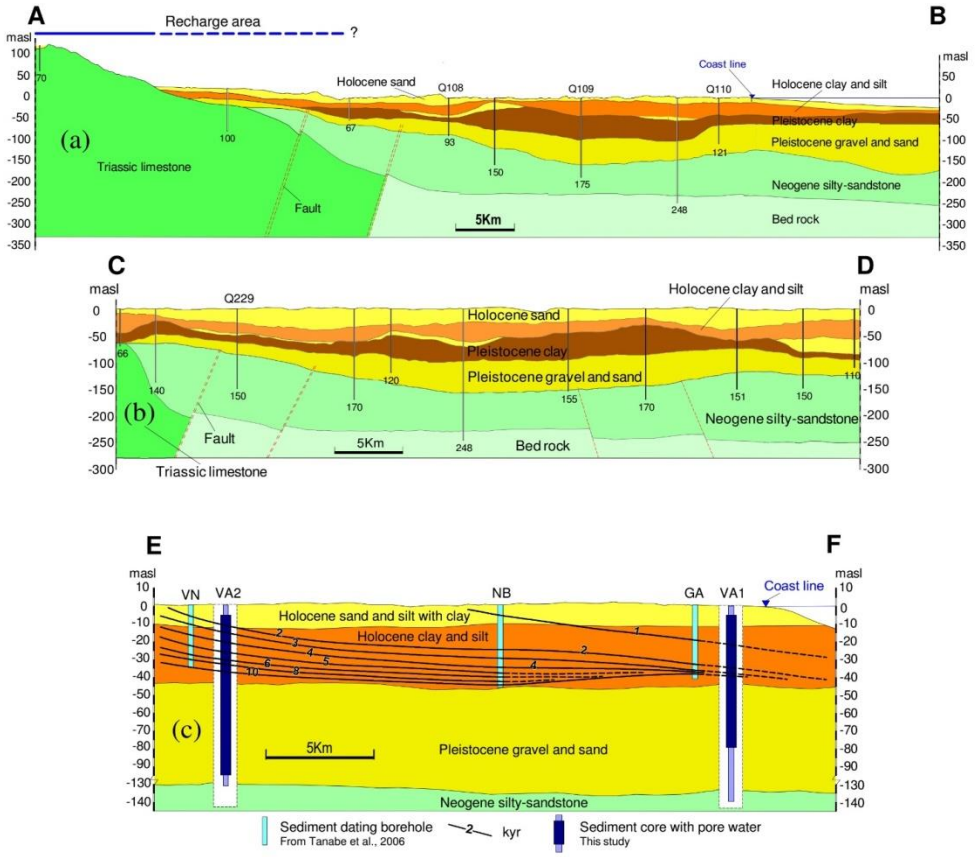

Figure 2. The subsurface geological in the Nam Dinh province as displayed in three cross-sections cutting the area as indicated in Fig. 1. Note that the vertical exaggerations are different in the three sections. Sediment ages in 2c are from Tanabe et al. (2006)

The hydrogeology of the Nam Dinh province is characterized by a Holocene upper sandy to silty, mostly unconfined aquifer, composed of the delta front sediments. The sandy layer is in a hydraulic relationship with the drainage canals and shallow river distributaries. The Early Holocene and Late Pleistocene clay layers act as aquitards, separating the shallow unconfined Holocene aquifer from the more deep, confined aquifer in the Pleistocene deposits. The coarse-grained Pleistocene regional aquifer is recharged at the limestone outcrops towards the west. Artesian condition in the aquifer was reported in the coastal zone during pristine conditions, and groundwater must have been flowing offshore as freshwater has been observed in Pleistocene layers in deep boreholes drilled off the shoreline. When fractured, the Triassic limestone and the Neogene silty-sandstone are aquifers in hydraulic relationship with the Pleistocene aquifer.

In the Nam Dinh province, growing rice in paddy fields occupies most of the land surface, and rice is harvested twice a year. Planting is done in the dry season in February and the rainy season in July. In the dry season, irrigation is done with surface water from a dense canal connected to upstream reservoirs. Rice planting at the beginning of the rainy season in July is, in most years, done without irrigation. The irrigation of paddy fields in the downstream part of the RRDP has an incomplete control effect on the groundwater table in the shallow aquifer systems.

3. Methods

3.1. Water depths and salinity measurements in the Red River

From the mouth of the Red River in the Gulf of Tonkin and up to 30 km upstream, measurements of water depth and salinity were done from small boats conducted in January and April. The endpoints of the survey lines are indicated in Fig. 3. The surveys were done in the dry season (in January 2009, April 2009, and April 2010), when seawater intrusions are expected to show maximum landward movement. Using a lead mounted with a heavy stone and a Diver® fixed to the end, water depths were measured from pressure readings, and salinities were obtained from electrical conductivity readings.

3.2. Collection of rainwater samples

Samples of rainwater representing average monthly values were collected in the Nam Dinh city to characterize water stable isotope composition. The method suggested by IAEA was followed (IAEA 2014). Water samples were stored in glass bottles until analysis was conducted.

Monitoring borehole and exploratory drilling:

Four existing deep boreholes and twelve newly drilled exploratory boreholes were included in this investigation for the location of these boreholes, as seen in Fig. 1. Boreholes are arranged in nests, where several holes have been drilled within a distance of meters, and separate screens have been installed in the high permeable Holocene, Pleistocene, and Neogene layers. The upper screens are typically 6 m long, while the deepest screens are 8-10 m. In the two exploratory boreholes VA1 and VA2 (Fig. 1), sediment sampling was collected using a wire piston coring device for laboratory experiments (Zapico et al., 1987). In addition, 21 new shallow exploratory boreholes were drilled into the near-surface delta front sediments, and these boreholes were screened in high permeable layers. For the location of these boreholes, see Fig. 3.

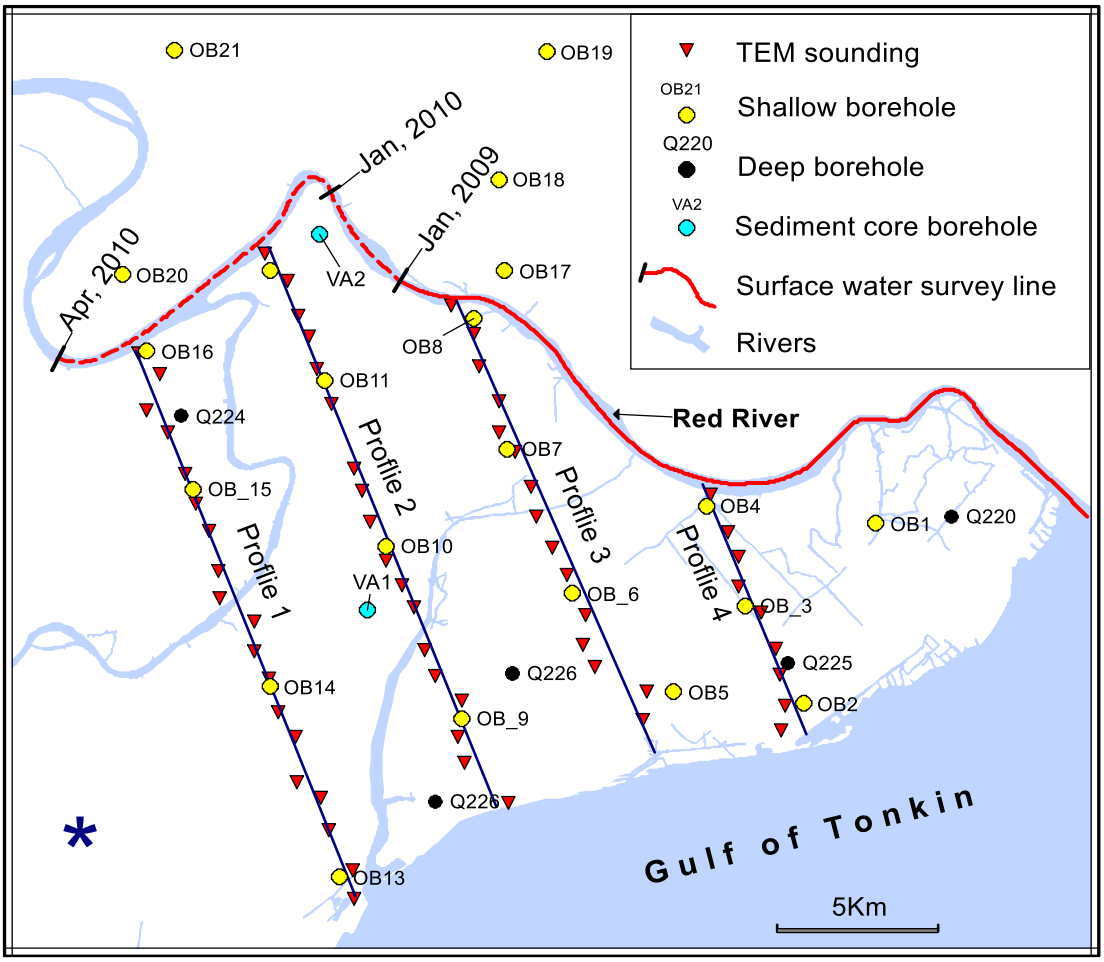

Figure 3. Detailed map showing the location of electromagnetic sounding, the location of the two exploratory boreholes (VA1 and VA2), and the three survey lines in the river, where water salinities have been measured

3.3. Measurement of groundwater heads

Hydraulic head variations were measured in 15 boreholes in the Pleistocene and 21 boreholes in the Holocene aquifers using Divers®. Historical manual measurements of the hydraulic heads in aquifers were obtained from the National Monitoring Programme.

3.3.1. Groundwater sampling and analyzing

In total, 33 groundwater samples were collected from shallow (Holocene aquifer) and deep boreholes (Pleistocene and Neogene aquifers) using submersible and Whale 12V pumps. With five times of water volumes in the borehole being flushed before water sampling, a flow cell equipped with probes for dissolved O_2, pH, and electrical conductivity (EC) was mounted directly on the sampling tube. EC and pH were determined after each emptied borehole volume to ensure that stable values were obtained simultaneously. The measurements were carried out with a WTW Multi 197i multi-purpose instrument using a WTW Tetracon 96 EC probe, a WTW SenTix 41 pH electrode, and for dissolved O_2, a WTW EO 196-1.5 cell electrode. Water samples were collected and filtered in 50 mL

syringes through 0.2 µm Sartorius Minisart cellulose acetate filters. Stable isotopic samples were not screened. Fe(II) and phosphate and silica were measured Spectrophotometrically with ferrozine (Stookey 1970), molybdate blue, and ammonium molybdate methods, the limit of detection was 1.8, 1.1, and 0.5 µM.

3.3.2. Geophysical borehole logging

Geophysical borehole logging was done simultaneously with water sampling to obtain information about the vertical distributions of salinities inside aquifers and interlaying aquitards. Geophysical borehole logging was done in the holes indicated in Fig. 1. A Robinson Research Ltd. Geologging Equipment was used, and electrical conductivities of formation and the sediment's natural gamma radiation for identification of lithologies (e.g., sand and clay) were measured. Electrical conductivities of formation were measured inside the PVC casings using a focused induction probe, which has a formation penetration depth of approximately 5 m. Formation electrical resistivities (ρ_f), expressed in Ωm, were calculated from measured formation conductivity (σ_f), expressed in [mS/m], using Equation 1.

$$\rho_f * \sigma_f = 1000 \quad \text{or} \quad \rho_f = \frac{1000}{\sigma_f} \qquad (1)$$

3.3.3. Transient electromagnetic soundings

As results from groundwater sampling and borehole logging only yields point information about the salinity distribution in the subsurface, transient electromagnetic sounding (TEM) was done, as this method earlier has proved suitable for mapping the distribution of salty, highly conductive layers in coastal aquifers (Stewart 1982; Fitterman and Stewart 1986; Mills et al. 1988; Tran et al. 2012). A total number of 61 TEM-sounding data were measured along four profiles located between the Red River and the coastline (Fig. 3). For details regarding data collection, processing, and interpretation, see Tran et al. (2012). The initial TEM data processing, i.e., editing of data and assignment of data uncertainties, was done with the SiTEM/SEMDI software (Auken et al. 2002). Subsequently, the TEM data were inverted profile to obtain 1-D resistivity models of the subsurface using a laterally constrained inversion (LCI) scheme, as Auken et al. (2005) described. The constraints can be seen as an a priori value for the expected geological variations between soundings.

3.3.4. Laboratory work

Water samples from boreholes and squeezed pore water from sediment cores were analyzed as follows: Samples for the cations: Na^+, K^+, Ca^{2+}, and Mg^{2+} were preserved with 2% of a 7 M HNO^3 solution and refrigerated until analyzed by flame absorption spectrophotometry on a Shimadzu AAS 688 instrument. Samples for Cl^-, NO^{3-} and SO_4^{2-} were collected in polypropylene vials and frozen immediately after sampling. The anions were analyzed by ion chromatography using a Shimadzu LC20AD/HIC-20ASuper. Due to high salinities in the samples, up to 250-fold dilution was required. A18 MΩ deionized water was used in the dilutions.

Using a Reeburg (1967) type squeezing device, a high pressure (N2) was applied to extract pore water from 22 cm long and 48 mm in diameter sediment core samples. The used N2 pressure was adjusted to the water content of the core samples. The water from each core sample varied between 20 and 40 ml. Immediately after sampling, the pore water samples were filtered through a Sartorius Minisart cellulose acetate filter (0.45 µm), and analyses resembled the procedure in the field. Water samples were also analyzed for major ions and stable water isotopes.

Pore-water stable isotope ratios of oxygen ($^{18}O/^{16}O$) and hydrogen (D) ($^2H/^1H$) were

measured relative to the VSMOW standard were analysed using a Picarro Cavity Ring-Down Spectrometer (CRDS) equipped with an autosampler and a vaporiser. The results are expressed in ‰ units using the δ-notation with standard deviations not larger than ±0.2‰ ($\delta^{18}O$) and ±0.5‰ (for $\delta^{2}H$), as calculated from four replicate injections into the vapouriser.

3.3.5. Textural, mineralogical, and hydraulic investigation of Holocene aquitard sediments

Two samples from the investigation borehole VA1 and two from VA2 were selected for examination of textural composition, clay mineralogical, and hydraulic properties. The grain size distribution of the sediment samples was determined using the standard sedimentation method.

For the preparation of samples for X-ray diffraction, the samples were dispersed in distilled water by ultrasonic treatment and the fraction < 2 μm was collected by separation in a continuous flow centrifuge. The X-ray diffraction was carried out in a Philips 1050 goniometer with CoKα-radiation obtained with a β-filter (Fe) and pulse height selection. Randomly oriented specimens were run to reveal minerals phases. Oriented clay specimens were prepared by sedimentation onto glass slides, and specimens that were Mg-saturated and air-dried, Mg-saturated and glycolated, Mg-saturated and glycerol saturated, K-saturated and air-dried, and K-saturated and heated to 300°C, were investigated. Oriented specimens were run with divergence and an anti-scatter slit of ¼ degree and with 10s per 0.1° 2θ.

Following the freezing of the retrieved sub-cores, cylindrical samples (plugs) of 1½″ in diameter were drilled using air as coolant. Darcy experiments were done on four intact plugs, with lengths of 5.0 cm and diameters of 3.7 cm, with well-defined constant hydraulic gradients and flows. The plugs were mounted in Hassler-type core holders and put under a confining hydrostatic pressure of 2 bar. Even though the samples were retrieved from different depths in the formation, it was chosen to use the same confining pressure for all samples. After settling, the samples were flooded with a 3% NaCl solution, and differential pressure and flow rate were measured continuously in order to enable the calculation of the hydraulic conductivity by application of Darcy's equation. Following the determination of the hydraulic conductivity, the influent was switched to tap water, and effluent water samples for EC measurements were collected continuously. When the EC in the effluent had stabilized, the effective porosity of each sample was calculated as the 50% mass breakthrough on the basis of the obtained breakthrough curve.

3.3.6. Solute-transport modelling

Solute-transport modeling was performed to simulate the leaching of marine pore water from the delta sediments for 10,000 years (10 ka). This was done in a two-dimensional cross-section following the geological cross-section in Fig. 2c, and the overall assumed pristine paleo- groundwater flow direction towards the sea. The main objectives of the modeling were to evaluate (1) transport mechanism of the saltwater out of the high and low permeable formations, whether a density controlled or diffusive transport has been prevailing, (2) to simulate the time the leaching of marine pore water will take in a geological time perspective. The SEAWAT (Guo and Langevin 2002; Langevin and Guo 2006) code for simulation of flow with variable density was used. SEAWAT couples the two commonly used codes MODFLOW (McDonald and Harbaugh 1988) and MT3DMS (Zheng and Wang 1998), with a variable density and viscosity package.

4. Results and interpretations

4.1. Salinity in the Red River

Measurements in the Red River in January 2009 showed salinities up to 50% of seawater

at a distance up to 16 km from the Gulf of Tonkin and 10% ocean salinity up to 26 km from the mouth of the river (Fig. 4). Vu (1996) reported similar salinity intrusion lengths of about 20 km in the Red River, and these observations have been confirmed by Pham (2004). For comparison, Zhang et al. (2013) report a maximum saltwater intrusion length of 78.3 km in the Pearl River and in the Mekong River, salty water has been observed up to 50-60 km inland (Nguyen et al., 2008). The main controls of the saltwater intrusion lengths in the rivers over the year are mainly changes in river discharges, tidal effects, and storm events during typhoon passages.

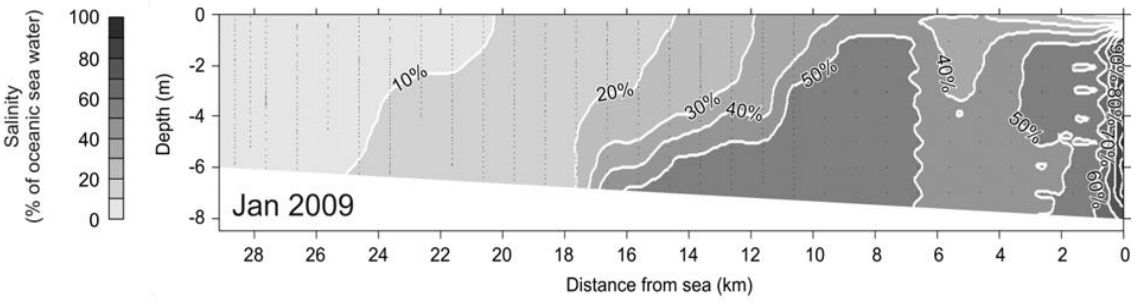

Figure 4. Water salinities in the Red River, as interpreted from measured eater electrical conductivities in January 2009. The salinity is given as percentages of the salinity in oceanic water

Saltwater intrusion from the Red River into the shallow aquifer in the Nam Dinh province is enhanced by sand excavations of sandy river bottom sediments, thereby maintaining good hydraulic contact between the river and the shallow aquifer. Therefore, it seems safe to conclude that a saltwater intrusion into the shallow aquifer in the Nam Dinh province will occur when a hydraulic gradient is established from the river into the aquifer (see next section). Still, salt transport can even happen against the upward hydraulic gradient due to the density contrasts between freshwater in the aquifer and dense salty river water.

4.2. Hydrogeology in the Nam Dinh province

Groundwater head elevations in the shallow, unconfined sandy aquifer are between -0.6 and +1.2 masl, with seasonal variations controlled by recharge and interactions with irrigation canals and river distributaries. Observed heads in three boreholes are depicted in Fig. 5. They show groundwater tables above the water stage, at approximately 0 masl close to the sea, in the Red River in the rainy season from June to October and a decreasing water table from the onset of the dry season in October. A high phreatic water table is re-established in the shallow aquifer from January/February after opening irrigation gates, and water flows into paddy fields. Gates have also been installed to prevent saltwater intrusion from the sea, and therefore the canals form a closed hydraulic system. Pumping from canals for irrigation in the dry season can cause the water stages in the river and phreatic water table to fall below sea level (Fig. 5), which further increases the risk of a saltwater intrusion from the Red River.

In the deep Pleistocene aquifer, the groundwater hydraulic head is strongly influenced by groundwater abstraction. The most significant drawdown around the central abstraction point is 25 km south of Nam Dinh (Fig. 6). Before groundwater abstraction in 1996, the hydraulic head in the major part of the Nam Dinh province was around +1 masl. Still, at the wellfields, close to observation borehole Q109, the groundwater level in the Pleistocene aquifer has been lowered to an elevation of 8 mbsl with a decline of about 0.5 m/year (inset in Fig. 6). Although smaller, the

drawdown in the Neogene aquifer is of the same size, indicating a hydraulic connection between the two aquifers with an upward leakage to the Pleistocene aquifer. In borehole Q110, located between the pumping wells and the coastline, the water table has been lowered from 1 masl to 6 mbsl, and an intrusion of salty water might therefore have been initiated. After pumping, a vertical downward hydraulic gradient across the up to ~90 m thick marine clays has been built up, reaching 160‰ in the central part of the cone of depression.

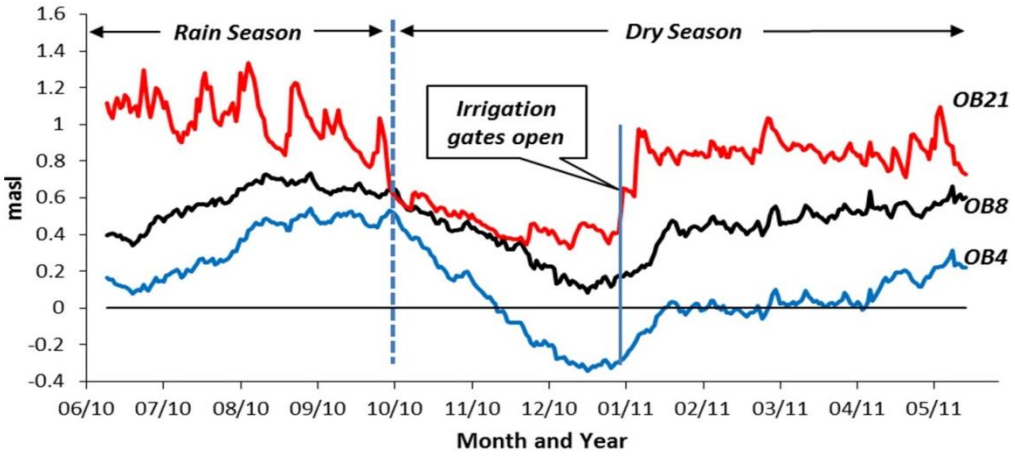

Figure 5. Hydraulic heads in three boreholes with screens in the shallow Holocene sandy aquifer. For location of the boreholes, see Fig. 3

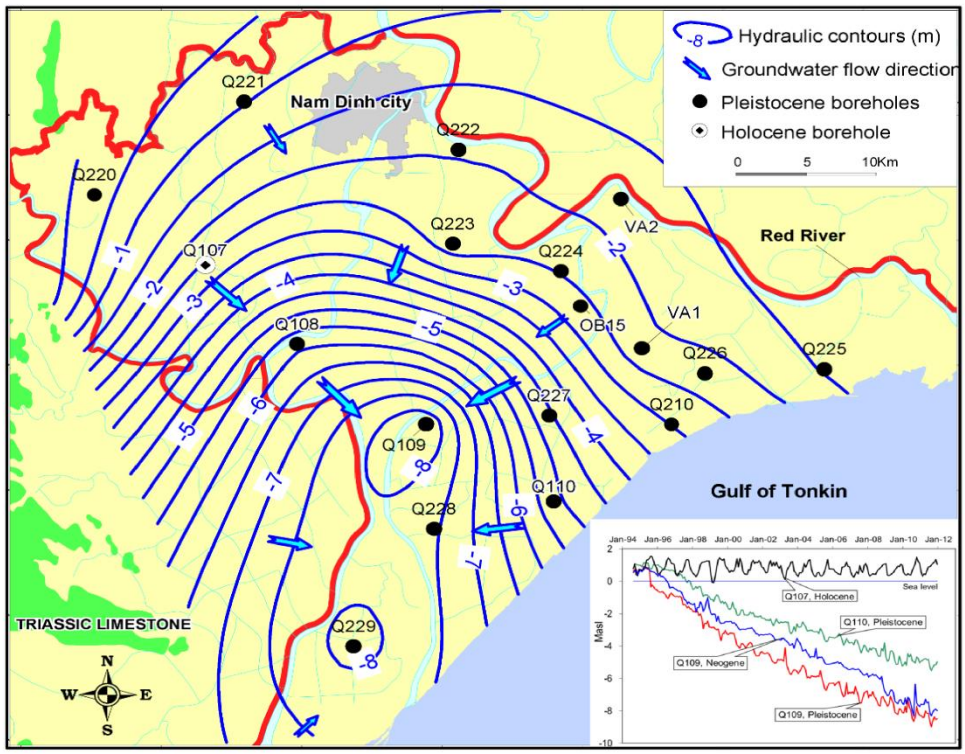

Figure 6. Hydraulic head distribution and groundwater flow direction in the Pleistocene aquifer. In the insert, historical head data from the shallow aquifer (Q107), the Pleistocene aquifer (Q109 and Q110) and the Neogene aquifer (Q109) are shown

Before the groundwater abstraction, the hydraulic heads in both the upper (Q107, Holocene) and lower aquifers (Q109, Pleistocene) were in this part of the province, both at 1 masl (see inset in Fig. 6). However, the hydraulic interaction between the two aquifers should have been limited during pristine conditions.

4.3. Groundwater chemistry

In the shallow sandy aquifer, high groundwater salinities have been observed close to the sea with TDS up to 17 g/L; the groundwater salinity decreases inland with values adjacent to the Red River of 5 to 6 g/L (Fig. 7). The highest salinities close to the sea strongly suggest saltwater intrusion from the sea. In contrast, the contribution to the TDS in the groundwater inland may come from an interaction with the dense network of drainage canals and rivers. Chemical analysis shows that groundwater in the shallow aquifer is anoxic, without nitrate, and with dissolved ferrous iron up to 38.5 mg/L (Table 1). Concentrates of sulfate are low, even in the water showing a high chloride concentration, and sulfate reduction must have occurred. The reducing character of the shallow groundwater must be explained by a high reactivity of the organic materials in the shallow marine sand (Postma et al., 2007). The highest chloride concentration of 11,236 mg/L (~ 60 % sea-water) is observed in borehole OB13, and the lowest Chloride concentration of 9 mg/L was observed in borehole OB19. The water composition and the salinity distribution in the shallow aquifer may be interpreted as a result of mixing of recharged fresh water from the surface and the irrigation canals, leakage of saltwater from the river distributaries, and upward diffusive transport from the underlying marine clay layers see later.

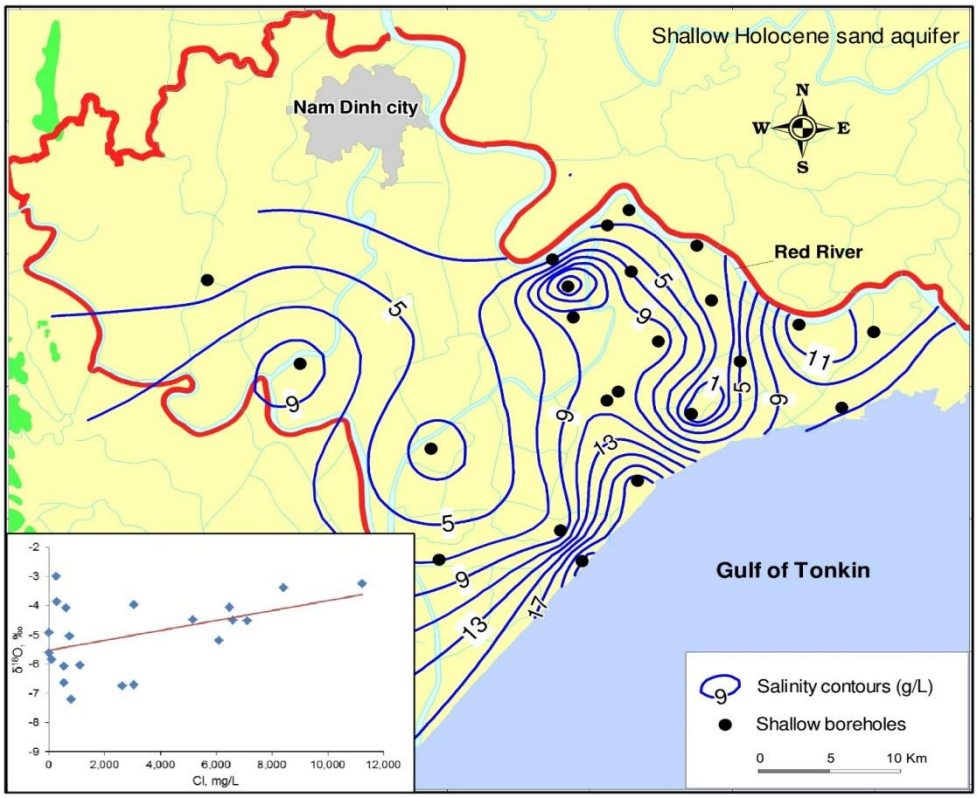

Figure 7. Measured total dissolved solids in the shallow, Holocene aquifer. Concentrations of chloride and water stable isotope compositions are given in the inset

Table 1. Groundwater composition in shallow boreholes

Borehole No	Depth m	Field data							Laboratory data										
		Ec	T	pH	O_2	Fe(II)	PO_4	HCO_3	Na	K	Ca	Mg	Cl	SO_4	Br	NO_3	F	$\delta^{18}O$	δ^2H
		mS/cm	°C		mg/L														
OB1	7.6	22.5	25.2	7.46	0.2	18.8	2.6	777.8	3864.6	108.9	54.8	300.5	7113.2	0.6	24.2	0.0	0.4	-4.53	-29.35
OB2	8.5	32.0	25.7	7.39	0.2	38.5	0.6	427.0	5503.9	99.7	238.7	482.2	5171.7	0.6	36.2	0.0	0.2	-4.48	-28.75
OB3	59.5	10.2	26.4	7.1	0.2	20.6	1.8	588.7	1438.1	28.6	130.4	128.7	3044.7	0.2	9.8	0.0	0.1	-6.72	-45.75
OB4	8.3	36.3	24.7	8.04	0.2	5.3	2.1	585.6	6097.0	199.0	45.3	511.6	8411.1	0.4	49.6	0.0	0.7	-3.39	-21.58
OB6	6.7	9.4	25.0	7.88	0.3	1.9	3.0	930.3	1692.8	74.6	32.9	148.6	2642.5	0.3	8.9	0.0	0.3	-6.76	-44.24
OB7	7.3	1.5	25.4	7.44	0.3	12.8	1.4	844.9	165.3	23.7	68.9	55.3	110.4	11.9	0.5	0.0	0.2	-5.85	-38.87
OB8	8.1	2.6	25.2	7.24	0.3	15.5	2.0	841.8	364.9	20.0	52.1	62.0	536.5	0.2	2.1	0.0	0.1	-6.07	-41.93
OB9	6.1	0.2	26.1	7.34	0.1	3.4	0.2	143.4	3.2	1.5	26.8	5.4	3.3	8.2	0.0	0.0	0.1	-5.61	-31.50
OB10	8	21.0	25.8	7.62	0.1	11.6	4.4	1525.0	3344.8	147.3	73.9	392.5	6101.2	0.6	20.1	0.0	0.5	-5.19	-35.52
OB11	7.8	11.4	25.5	7.79	0.1	1.7	5.4	1433.5	1951.7	90.2	43.5	188.6	3047.0	0.4	10.5	0.0	0.3	-3.98	-29.41
OB12	7.6	4.3	25.8	7.48	0.1	13.2	1.4	817.4	680.9	35.8	77.2	95.8	1117.7	0.2	3.9	0.0	0.1	-6.03	-41.54
OB13	6.7	38.7	25.4	7.64	0.1	8.7	3.8	2000.8	6424.6	220.1	129.3	679.6	11236.0	3.8	65.8	0.0	0.5	-3.25	-21.90
OB14	8.4	21.7	24.3	7.53	0.5	5.2	5.6	1403.0	3392.2	141.7	47.5	305.0	6482.2	0.6	21.3	0.0	0.5	-4.06	-27.47
OB15	8.8	6.9	28.7	7.02	0.4	29.4	1.5	756.4	962.4	29.0	121.5	97.2	735.6	0.2	2.9	0.0	0.0	-5.06	-34.50
OB16	9.6	1.8	25	7.51	0.1	2.5	2.3	771.7	207.4	38.2	44.8	82.8	274.8	0.1	0.9	0.0	0.4	-3.88	-29.04
OB17	13.8	21.2	28.1	7.65	0.3	7.3	5.7	1274.9	3544.2	149.7	33.8	301.8	6596.4	0.2	21.9	0.0	0.4	-4.50	-30.39
OB18	7.1	2.8	24.7	7.88	0.2	1.7	1.4	634.4	408.3	29.2	46.0	68.9	630.3	0.4	2.2	0.0	0.2	-4.08	-27.71
OB19	7.4	0.3	25.7	7.14	0.1	21.8	0.4	158.6	17.9	5.1	14.0	5.7	9.1	0.1	0.0	0.0	0.1	-4.92	-33.97
OB20	6.5	2.4	25.2	6.93	0.2	36.7	1.5	555.1	154.9	9.9	161.8	51.5	536.8	0.2	2.3	0.0	0.1	-6.64	-45.30
OB21	7.9	1.7	23.8	7.45	0.8	2.8	1.1	603.9	152.3	35.2	51.3	81.6	267.3	0.4	0.9	0.0	0.5	-3.00	-19.84
VA2a	15	330.0	nd	7.5	ND	8.7		695.4	484.4	15.1	123.8	50.3	792.7	0.2	3.1	0.0	0.1	-7.21	-48.34

In the Pleistocene aquifer, groundwater TDS values up to 6 g/L are observed close to the Red River. Groundwater salinities decrease towards the center of the cone of depression, where groundwater with TDS values below 1 g/L is present. Relatively low TDS is also encountered upstream, towards the recharge area towards the west (Fig. 1).

The Pleistocene aquifer is anoxic, with elevated concentrations of dissolved ferrous iron up to 25 mg/L and sulfate concentrations below 1 mg/L (Table 2), indicating ongoing sulfate reduction. The highest concentrations of sulfate (8.5 mg/L) are found in the borehole Q227, where groundwater is fresh, as noted in a chloride concentration of 8.9 mg/L. Groundwater in the Pleistocene aquifer may be interpreted as mixing of a Ca^{2+}-HCO_3^- freshwater type and a modified marine Na^+-Cl^- water type, affected by the reduction of sulphate and cation exchange.

Table 2. Groundwater composition in deep boreholes

Borehole No	Depth m	Field data							Laboratory data										
		Ec	T	pH	O_2	Fe(II)	PO_4	HCO_3	Na	K	Ca	Mg	Cl	SO_4	Br	NO_3	F	$\delta^{18}O$	δ^2H
		mS/cm	°C		mg/L														
Q223	106	293	28.6	6.71	0.13	17.1	0.2	222.7	297.6	6.7	150.3	50.6	845.8	0.3	2.9	0.0	0.1	-8.23	-58.37
Q223	138	285	28.5	6.52	0.05	25.2	0.3	183.0	329.6	5.3	127.5	56.4	863.4	0.2	2.8	0.0	0.1	-8.57	-60.52
Q224	100	294	28.6	6.9	0.11	20.0	0.4	271.5	304.9	7.7	144.0	61.9	823.7	0.3	2.8	0.0	0.1	-7.65	-54.62
Q224	45	2360	nd	7.63	0.32	7.2	2.9	1256.6	7195.2	219.4	122.2	674.0	8407.8	0.5	31.2	0.6	0.0	-3.20	-21.66
Q225	110	608	27.9	7.3	0.11	2.1	0.1	542.9	984.7	28.6	97.0	107.4	1804.2	0.4	6.0	0.0	0.1	-7.31	-49.99
Q225	67	512.8	25.4	8.22	0.37	0.6	0.3	622.2	850.5	26.4	58.8	90.7	1428.5	0.3	4.8	0.1	0.1	-7.33	-50.66
Q226	104	368	nd	7.26	0.14	7.8	1.3	469.7	581.2	13.4	73.8	52.0	1014.1	0.2	3.4	0.0	0.1	-7.63	-51.69
Q226	151.5	274	29.5	7.99	0.14	5.9	0.2	366.0	321.4	10.2	107.2	81.1	744.7	0.2	2.6	0.1	0.1	-7.65	-52.35
Q227	155.5	0.453	29.3	7.7	0.13	0.2	0.4	311.1	56.2	4.7	21.2	18.3	8.9	8.5	0.0	0.0	0.2	-7.47	-52.77
VA1	132	340	29.4	6.88	0.1	9.0	0.3	295.9	382.0	8.9	92.6	66.6	793.2	0.2	2.7	0.0	0.1	-7.37	-50.59
VA2	139	1405	28.2	7.04	0.12	15.4	2.3	500.2	2085.5	58.2	221.0	206.5	4156.0	1.1	17.9	0.0	0.2	-6.50	-45.67
OB15	95	1.156							122.9	8.6	38.1	34.2	244.8	0.1	0.9	0.0	0.1	-7.48	-51.32

nd = no data

4.4. Water stable isotope compositions

Rainwater sampled in Nam Dinh during 2011 shows $\delta^{18}O$ values between -11.9 and -2.5 ‰, and δ^2H between -88.1 and -6.8 ‰, with a relationship described by the equation $\delta^2H = 8.4\delta^{18}O + 15.2$ ($R^2 = 0.98$), see Fig. 8. This local meteoric water line is close to the global meteoric water line ($\delta^2H = 8.13\delta^{18}O + 10.8$)

suggested by Rozanski et al. (1993), but displays a larger deuterium excess value (Clark and Fritz, 1997). Looking at the rainwater stable isotope oxygen composition through the year, rainwater in the dry season shows a relative enrichment with values up to -2.5‰, whereas during the rainy season from June to October, values are between -12 and -8‰ (Inset in Fig. 8). A similar yearly variation in RRDP precipitation has previously been reported from Hanoi (Larsen et al., 2008). The phenomena may be ascribed to the effect reported in Southeast Asia. (Dansgaard 1964). In groundwater from the shallow aquifer, the relationship between the stable oxygen and hydrogen isotopes composition is described by the equation $\delta^2H = 6.6\delta^{18}O - 0.8$, and the $\delta^{18}O$ composition varies with a relatively large variation between -7.5 and -3.0 ‰ (Fig. 8). These significant variations in the water stable isotope composition can be either from enrichment by evaporation of surface water or from mixing with seawater. The relationship between $\delta^{18}O$ and chloride in groundwater from the shallow aquifer (Inset in Fig. 8) shows a mixing line with chloride values between 0 and 12,000 mg/L, with enrichment in the water stable isotope composition with increasing salinity of the water. However, a significant variation in the water stable oxygen composition is also seen in the water with low concentrations of chloride, which may be explained by enrichment due to evaporation of fresh water in surface water bodies. The relatively large $\delta^{18}O$ variation in the shallow groundwater might be further accentuated by infiltration of local rainfall with large $\delta^{18}O$ variations during the year (2011) as seen in the Nam Dinh rainwater (inset in Fig. 8).

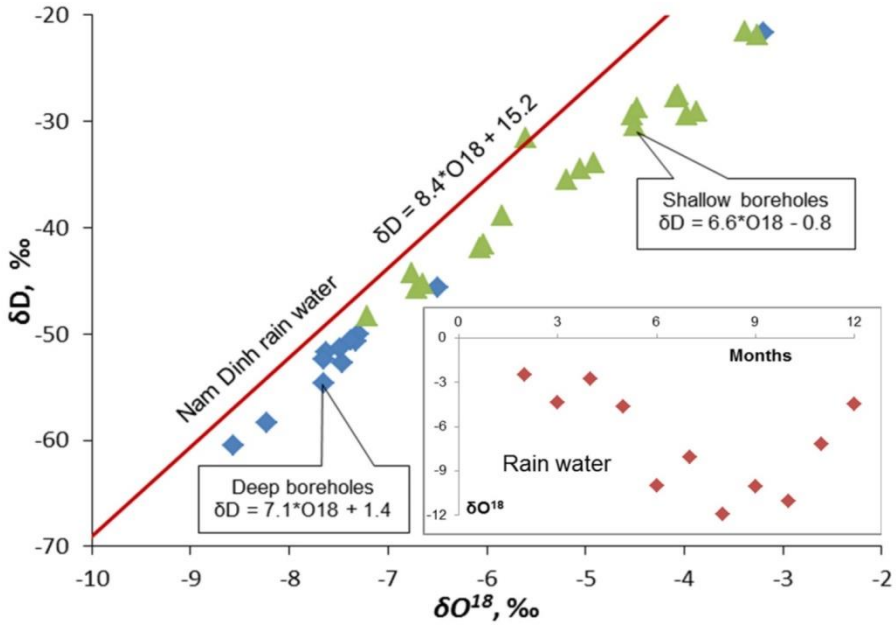

Figure 8. The stable water isotope composition in rain water and groundwater in the Nam Dinh province. Variation in the $^{18}O/^{16}O$ stable isotope composition in rainwater through 2011 is shown in the inset

Groundwater from the Pleistocene aquifer shows a relationship between the water stable isotopes given by the equation $\delta^2H = 7.1\delta^{18}O + 1.4$, and apart from one high salinity sample, the $\delta^{18}O$ composition varies within a relatively narrow interval of from -8.5 to -6.5‰ (Fig. 8).

The water's relatively constant stable isotope value in Pleistocene groundwater

should reflect a more constant recharge source in the outcropping limestones, where a rapid infiltration takes place without a secondary enrichment from evaporation. The water stable isotope data clearly shows that with the different isotopic fingerprints in the two aquifers, the water interactions between the shallow and deep aquifers in the delta sediments have been minimal without any significant groundwater mixing.

4.5. Borehole geophysical logging

As revealed from the geophysical borehole logging, the vertical distribution of salinities in the Quaternary sediments in the Nam Dinh province can be summarized with results from five boreholes as depicted in Fig. 9. The interpretation of these results has been supported with information from drilling, where intact coring of sediment (Wagner et al. 2011). The location of this (non-linear) cross-section with boreholes is depicted in Fig. 1. As revealed from the natural gamma radiations, the distribution of aquifers and aquitards shows that the uppermost ~10 m of delta front sediments appear in some of the boreholes as sandy and silty layers (boreholes Q221 and Q222). In contrast, in other boreholes, this unit consists of clay-rich layers (boreholes Q223, Q109, and Q110). Identified by high gamma radiation values, Holocene clay-rich, silty, and fine sand layers are found below the sand and down to 100 mbsl. Late Pleistocene clay is present in some boreholes (Fig. 9, boreholes Q109, Q110, and Q223), identified by a high gamma radiation reading. Still, this clay has relatively low formation conductivity (more discussion will be presented in the next section). The underlying layers with a relatively low natural gamma radiation represent Pleistocene gravel and sand deposits, overlying Neogene siltstone and sandstone as seen in boreholes Q221 and Q223 (Fig. 9).

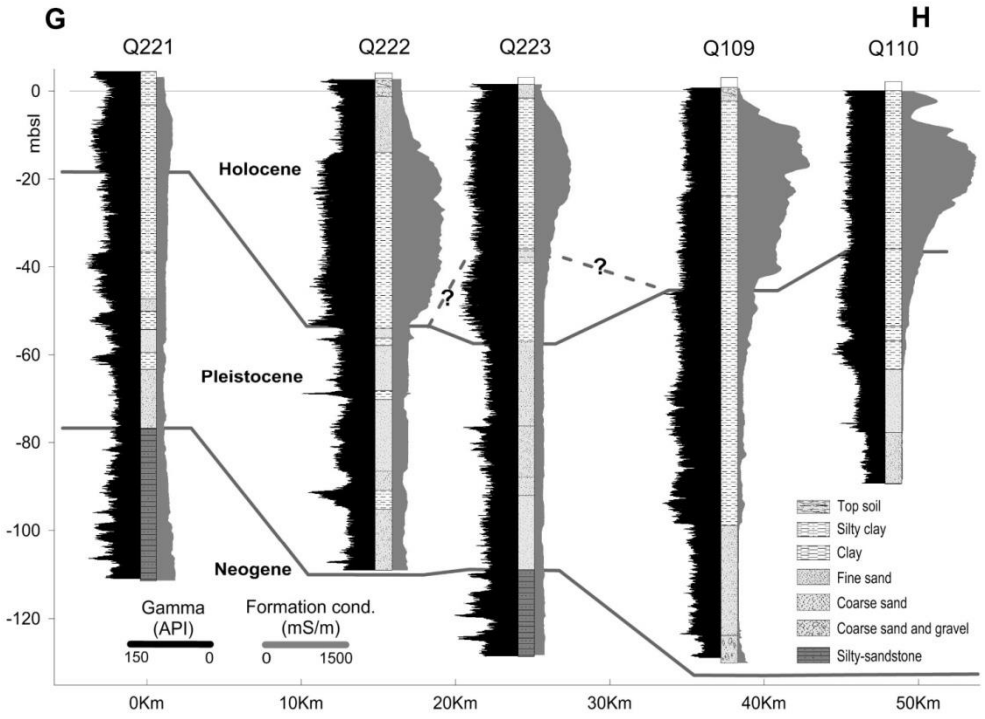

Figure 9. Geophysical logs from five selected borehole in the Nam Dinh province. For the location of boreholes, see Fig. 1

In some of the boreholes, measured formation conductivities in the upper delta front unit show elevated formation conductivities in the bottom of shallow sandy layers (e.g., borehole Q222 in Fig. 9). As interpreted from the continuous natural gamma radiation, this shape in the formation conductivity, combined with relatively constant sand/clay content, indicates high saline groundwater present at the shallow aquifer's bottom. A formation conductivity of 500 mS/m corresponds to a water conductivity of 2,000 mS/m, assuming a sand formation factor of 4, or 35 - 40 % of the conductivity of seawater.

In the clay-rich Holocene aquitard, measured formation conductivities are typically between 500 and 1,000 mS/m, with a measured peak value at 15 mbs of 1,350 mS/m (~0.7 Ωm) in borehole Q109 (Fig. 9). With the almost constant natural gamma radiation in this formation, the exceptionally high electrical formation conductivities may be explained by the occurrence of highly saline pore water rather than lithological heterogeneities. Measured formation conductivities in the Holocene aquitard show consistently increasing values towards the sea, reflecting an increasing salinity towards the sea. Holocene aquitard layers overlie sandy Pleistocene deposits (Borehole Q222). The formation conductivity log is almost symmetrical, decreasing conductivity values towards the sandy layers. This spatial distribution of formation electrical conductivity could be interpreted as reduced salinities towards the sandy layers, controlled by a diffusive transport of salts out of the clay and adjacent sand layers. Where the aquitard material is overlying Pleistocene clay-rich layers (Borehole Q109, Q110, and Q223), asymmetrical log patterns are observed; interpreted to be an effect of diffusion, may be combined with density-driven transport. This interpretation implies that the originally marine pore water in the Pleistocene clays was leached out by freshwater during a low sea level period before the Holocene clay was deposited.

Measured borehole formation conductivities in the Pleistocene aquifer range from 20 to 300 mS/m, confirming the observed spatial distribution of salinities as revealed from the groundwater sampling (Fig. 1); with high concentrations close to the Red River and decreasing concentrations towards the groundwater abstraction locations. Based on laboratory studies, which will be discussed in the following section, the form factor in the very coarse-grained Pleistocene deposits can be estimated to a value of 2, implying that calculated groundwater conductivities resemble observed values in water samples from boreholes. Measured vertical conductivity logs show no indications of saltwater intrusion in the Pleistocene aquifer (Fig. 9, Boreholes Q109 and Q110). Still, it can be challenging to assess from these observations, as these boreholes have not been drilled to the bottom of the Pleistocene deposits.

4.6. TEM measurements

Results from the four TEM profiles display minor variations, and therefore, only profile 2 is shown (Fig. 10). The depth of investigation of the soundings is about 80 m, which is into the Pleistocene alluvial layers. Generally, three electrical units are seen on the profiles: An uppermost 2 to 10 m thick unit, with apparent resistivities from 5 and to 100 Ωm, which are interpreted to represent the shallow delta front layer containing either brackish or fresh groundwater, an underlying irregular second unit from 10 to 35-50 mbsl, with an apparent resistivity between 0.8 and 1.25 Ωm, representing the Holocene aquitard, and a lowermost unit with apparent resistivities typically between 7 and 15 Ωm. Lateral variations in the thickness of the very low

resistivity unit (Unit 2), must be interpreted to represent lithological changes and hence varying saltwater leaching from the clay-rich sediments. Formation resistivity value variations in the coarse-grained, homogeneous Pleistocene formation represent mainly variations in groundwater salinity.

4.7. Exploratory boreholes

Interpretations of groundwater salinities from apparent formation resistivities obtained from geophysical borehole logging and TEM surveys have confirmed results from the exploratory boreholes VA1 and VA2. Borehole VA1 is located within TEM profile 2, approximately 7 km from the sea, and was drilled to 132 mbsl into the Neogene sandstone. Borehole VA2 is about 17 km from the sea, and was drilled to 139 mbsl into the Neogene sandstone (Fig. 9, Fig. 10). Results from borehole VA2 show a significant similarity to those from VA1.

The intact sediment cores from borehole VA1 showed clay-rich layers with thin layers of silt and sand. The compositions of squeezed pore water from cores are shown in Table 3. A peak with a pore water chloride concentration of 15,286 mg/L at 16.30 mbsl corresponds to the salinity of approximately 80 % of seawater (Hoang et al., 2018). The EC of this water sample is 5,080 mS/m, and the calculated pore water resistivity is 0.2 Ω m. The data confirms the low formation resistivities below 1 Ω m in the TEM soundings at these depths in the formation (Fig. 10). A good correlation was found between measured chloride and pore water electrical conductivity (R = 0.9945). A comparison between measured pore water EC and formation resistivity yields a clay formation factor of 6.65. As mentioned, the calculated formation factor in the sandy Pleistocene deposits, based on formation and pore water conductivities, was close to 2. The stable isotope composition of the squeezed pore water shows δ^2H values between - 48 and -16‰ and $\delta^{18}O$ values between -7 and -2‰, with a relationship of $\delta^2H = 6.65\delta^{18}O - 2.75$. The enrichment of $\delta^{18}O$ up to - 2‰, where the highest saline concentrations of the pore water are seen, indicates the marine origin of this water. Seawater by definition has a δO^{18} water composition of 0 ‰ (Clark and Frits 1997), and the deviation from this value can be explained with a primary dilution of seawater by river freshwater (15,286 mg/L chlorides) or generation of ultrafiltration condition during squeezing, which generates isotopic fractionation with a lighter ultrafiltrate (Coplan and Hanshaw 1973). The fact that a peak with a composition corresponding to 80 % seawater is found in the aquitard, supports the conclusion that advective transport of meteoric water through the formation has not occurred after deposition of the sediments.

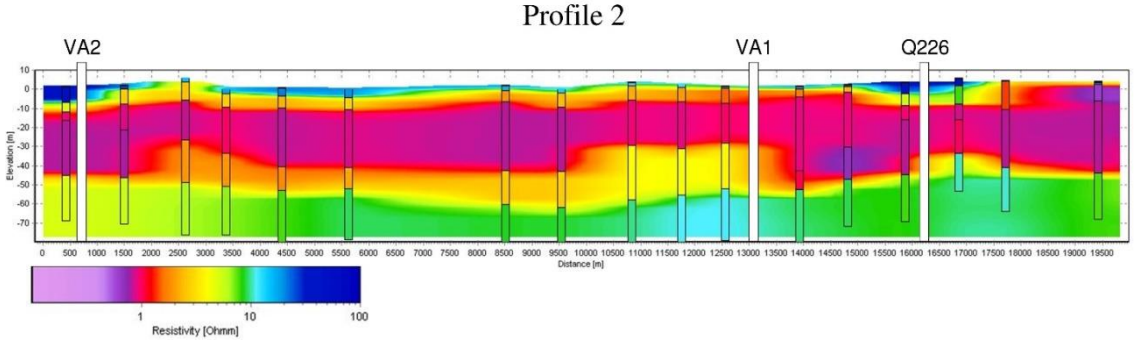

Figure 10. Cross-section with results of TEM soundings in Profile 2. The location of the profile is shown in Fig. 3. VA1 and VA2 are the locations of exploratory boreholes

Table 3. Pore water composition in clay layer in borehole VA1

Depth	EC	Na	K	Ca	Mg	NH_4	Si	Fe	Cl	Br	SO_4	PO_4	alk.	NO_3	NO_2	F	Total As	$\delta^{18}O$	$\delta^{2}H$
m	mS/m	mg/L															µg/L		
6.23	2112	NA	138	86	293	NA	14	0.29	5,251	22	19	2	729	13	18	4.2	69	-3.86	-30.2
11.22	4580	6,425	342	59	657	108	10	0.08	13,860	56	7	2	484	0	41	2.9	30	-2.27	-18.3
16.30	5080	6,875	346	60	703	NA	6	0.18	15,286	62	19	1	464	0	43	0.0	31	-2.06	-16.4
21.30	4320	6,737	411	NA	600	NA	10	0.03	12,587	51	9	2	558	0	34	4.0	30	-2.19	-15.7
26.80	3224	4,511	270	72	657	54	7	0.01	8,662	37	35	1	882	12	30	4.3	14	-2.95	-22.7
31.33	1763	2,510	173	132	439	48	16	0.03	4,610	18	17	0	770	10	0	2.4	10	-4.88	-34.6
36.50	826	862	88	85	208	60	15	0.00	2,119	9	25	0	473	0	0	2.5	15	-4.98	-38.9
41.75	331	335	17	167	50	NA	17	1.76	700	0	11	0	267	11	0	3.0	52	-6.51	-46
51.61	92	82	9	30	10	14	8	0.31	201	1	5	0	93	1	0	0.0	16	-6.87	-47.6
61.50	75	147	17	31	12	15	7	NA	119	0	3	0	107	1	0	1.0	30	-6.97	-48.4
71.28	78	112	12	36	13	8	NA	NA	NA	NA	NA	0	97	NA	NA	NA	6	-6.3	-46.6
81.50	141	NA	NA	NA	NA	NA	NA	NA	NA	NA	NA	0	51	NA	NA	NA	NA	NA	NA
91.00	140	576	57	35	16	10	NA	NA	NA	NA	NA	0	0	NA	NA	NA	12	NA	NA
95.70	102	137	38	NA	20	NA	5	NA	251	1	11	0	62	0	0	0.5	14	-6.77	-47.9

NA= not analysed

The overall water composition in the squeezed water from the marine clay show reduced water with a low concentration of sulfate, compared to the 2,800 mg/l presents in seawater. Ammonium concentrations are up to 108 mg/L, reflecting a decomposition of reactive, organic material in the sediments (Postma et al., 2007), and the content of nitrate and nitrite in the water may be formed during oxidation of the ammonium during sampling of pore water. The concentration of fluoride up to 4.3 mg/L reflects mineral reactions in the sediments, as the concentration of this element is only 1.3 mg/L in seawater.

4.8. Sediment sample results

Sediment samples from the Holocene aquitard are found dominated by clay (30-40%) and silt (57-68%), but sandy silt layers are also present where fine sand makes up 22% of the sediment (Table 4, sample VA2-2). The clay mineralogy is dominated by kaolinite and illite, formed by the decomposition of silica minerals, but vermiculite and smectite are also present.

Table 4 Textural, mineralogical and hydraulic properties of sediments from the Holocene marine unit. The samples VA1-1 and VA1-2 are from the exploratory borehole VA1. and the samples VA2-1 and VA2-2 are from borehole VA2. (+) indicates that the clay mineral might be present, (+) that the mineral is present in small amounts, (++) shows that the mineral is present and (+++) dominant clays in the samples

Sample	Depth	Grain size (%)			Clay Mineralogy					Hydraulic properties	
No		Clay	Silt	Fine sand	Kaolinite	Illite	Chlorite	Vermiculite	Smectite	K	Porosity
	(m)	(<2 µm)	(2-63 µm)	(63-200 µm)						(m/s)	(%)
VA1-1	20.80	42	57	1	+++	+++	-	+	++	$4.0 \pm 0.2*10^{-10}$	42 ± 1
VA1-2	35.70	31	68	0	+++	+++	(+)	+	+	$6.0 \pm 1.0*10^{-10}$	36 ± 1
VA2-1	21.40	39	60	1	++	++	(+)	+	++	$1.0 \pm 0.3*10^{-10}$	-
VA2-2	59.50	10	67	22	+++	+++	(+)	++	+	$4.5 \pm 1.0*10^{-9}$	36 ± 1

Hydraulic conductivities obtained in samples dominated by clay and silt are between 1.0 and 6.0×10^{-10} m/s, and the sandy silt has a hydraulic conductivity of 4.5×10^{-9} m/s. Estimated effective porosities of the sediments are from 36 to 42%. For comparison Bryant et al. (1975) reported results from unconsolidated marine sediments, with a clay content below 60% and porosity of 30-40%, having hydraulic conductivities in the range from 1 to 2.8×10^{-10} m/s. Based on studies of natural soft clays, Tavenas et al. (1983) concluded that the permeability of the sediments is controlled by the void ratio, the clay fraction, the plasticity index, and the clay's fabric anisotropy is negligible in marine clays. The very low

hydraulic permeabilities observed in this Holocene aquitard are most likely mainly controlled by the swelling clay smectite in the sediments. As fracturing in these clays is insignificant, the observed hydraulic properties can be seen as representative of the in-situ hydraulic properties of the Holocene aquitards in the field scale and comparable to observations from other studies.

4.9. Numerical modelling

The conceptual hydrogeological model applied in the numerical simulations of saltwater leaching (chloride leaching) during 10 ka is based on the geological cross-section shown in Fig. 2c. Late Pleistocene overlies the lower Pleistocene gravel and sand aquifer and Early Holocene marine clay and silt, superimposed by delta front sand constituting the shallow aquifer. In the model, the deposition during Early Holocene time follows the geological model suggested by Tanabe and co-workers (Fig. 2c). For the sake of simplicity, we assume the initial oceanic pore water composition in the Late Pleistocene marine clay (20,000 mg/L chlorides). However, borehole logging suggests that saltwater might have previously been leached out of the formation (see borehole Q109 in Fig. 9). The boundary between land and sea is set at the South-eastern (right) side of the model domain, with a constant chloride concentration of 20,000 mg/L. Consecutive simulation periods (stress periods) of 1 ka are used, and the thickness of the Holocene clay is increased with 1/10 of its total clay thickness in every simulation period. Inactive cells are activated when clay layers are incorporated in the model domain (Larsen et al., 2017). A prescribed head boundary is used at sea by applying the sea-level change in the Gulf of Tonkin during the last 10 ka. A prescribed head boundary was also used inland in the 40 km long profile, and was adjusted in each simulation period, to maintain a horizontal hydraulic gradient of 0.3‰. The groundwater-ocean interaction is controlled by the pressure difference across the sea bottom and the conductance of the aquitard bottom layers, which is fixed to obtain a vertical upward hydraulic gradient of 0.3‰. The hydraulic conductivity of the shallow and deep aquifer was fixed at 1×10^{-4} m/s and 3×10^{-4} m/s, respectively. The hydraulic conductivity of the clay was varied between 1×10^{-10} and 1×10^{-6} m/s, and the effective porosity was fixed at 10%. Groundwater forwarding into the model domain at the inland boundary contains 0 mg/L chloride.

Fig. 11 shows the results of simulations of leaching of the marine pore water with a hydraulic conductivity of the aquitard layer of 1×10^{-9} m/s at 5 ka, 3 ka, and 0 ka, corresponding to 5 ka, 7 ka, and 10 ka after the onset of the sedimentation of the aquitard sediments. These results reveal that at 5 ka, sediments in a 40 km wide zone from the present coastline were still dominated by marine pore water, while freshwater flushing had occurred in a 5 km wide area from the inland boundary. At 3 ka, flushing with freshwater had affected 10-15 km of the Pleistocene aquifer and 20 km of the Holocene aquifer. At 0 ka, corresponding to present, freshwater is shown in both the Pleistocene and Holocene aquifer. In contrast, in the Holocene clay, chloride concentrations are between 10,000 and 20,000 mg/L, in the same range as seen now in the Holocene aquitard. A simulation using a hydraulic conductivity of the Holocene aquitard of 1×10^{-8} m/s shows similar results.

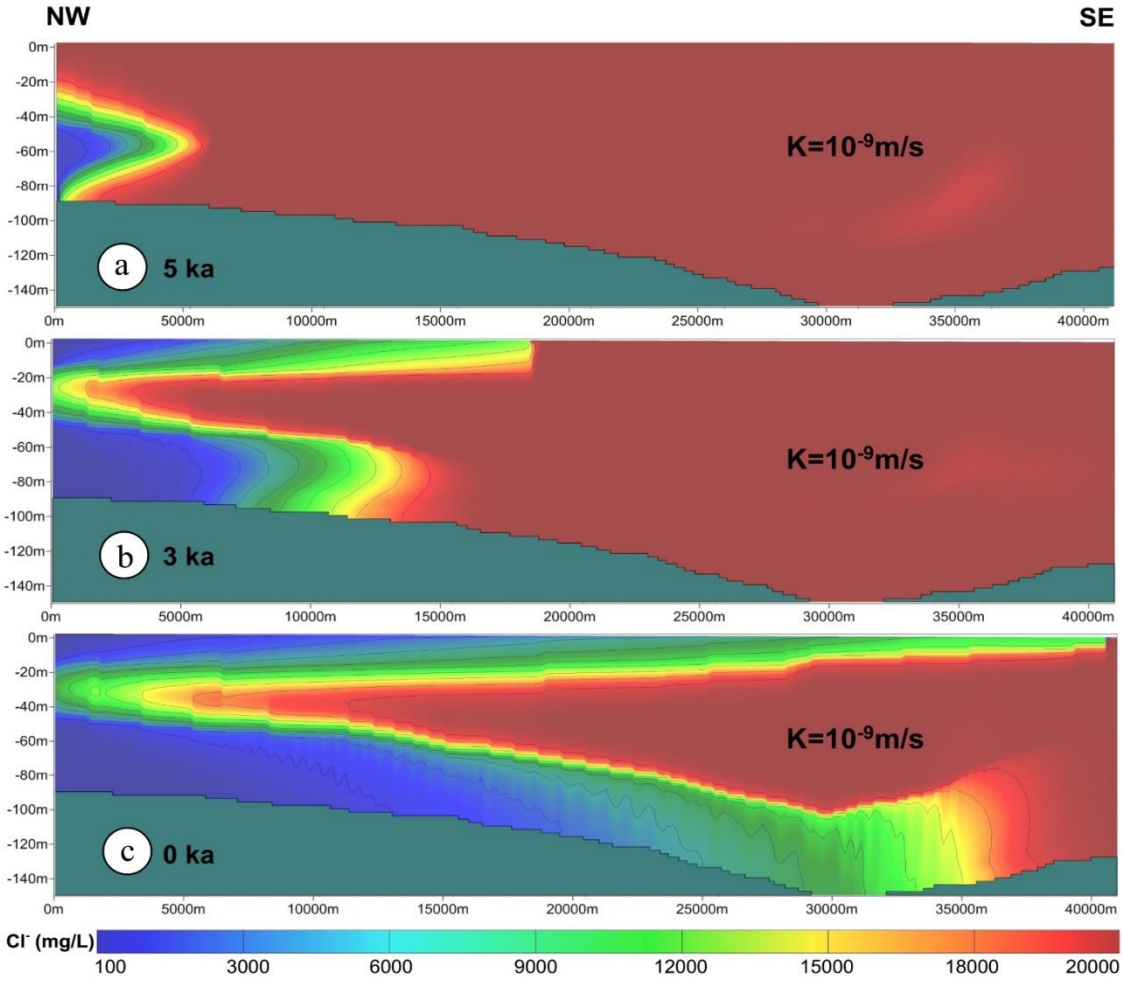

Figure 11. SEAWAT simulation results with hydraulic conductivity of the aquitard clay of 10-9 m/s. Initial concentration of chloride in the model domain is 20 g/L, ad results show concentrations after 5.000, 7,000 and 10,000 years of saltwater fluxing

In the simulations with a hydraulic conductivity of the Holocene clay of 10^{-7} m/s, relatively fast leaching of the marine pore water from both sand and clay was initiated about 4 ka, and at present (0 ka), freshwater has flushed the marine pore water from a large part of the model domain, and chloride concentrations up to 20,000 mg/L, is only seen in a zone up to 10 km from the coastline (Fig. 12). In the simulations with a hydraulic conductivity of the Holocene clay of 1×10^{-6} m/s, elevated concentrations of the saltwater is only seen in a zone up to 10 km from the coastline (Larsen et al., 2017).

This conceptual numerical modeling indicates that leaching by freshwater with an aquitard hydraulic conductivity below 1×10^{-8} m/s, Concentrations of chloride, and associated cations from seawater, will be present in concentrations comparable to observed concentrations in the Holocene aquitard. With higher hydraulic conductivities of the aquitard, the Holocene aquitard should now be dominated by freshwater, which is clearly in contrast to

our field observations. The explanation of the occurrence of salty groundwater in the model results at the coastline is likely to be affected by the applied boundary condition (constant pore water concentration of 20,000 mg/L), which is probably not realistic (more discussion can be found in the next section).

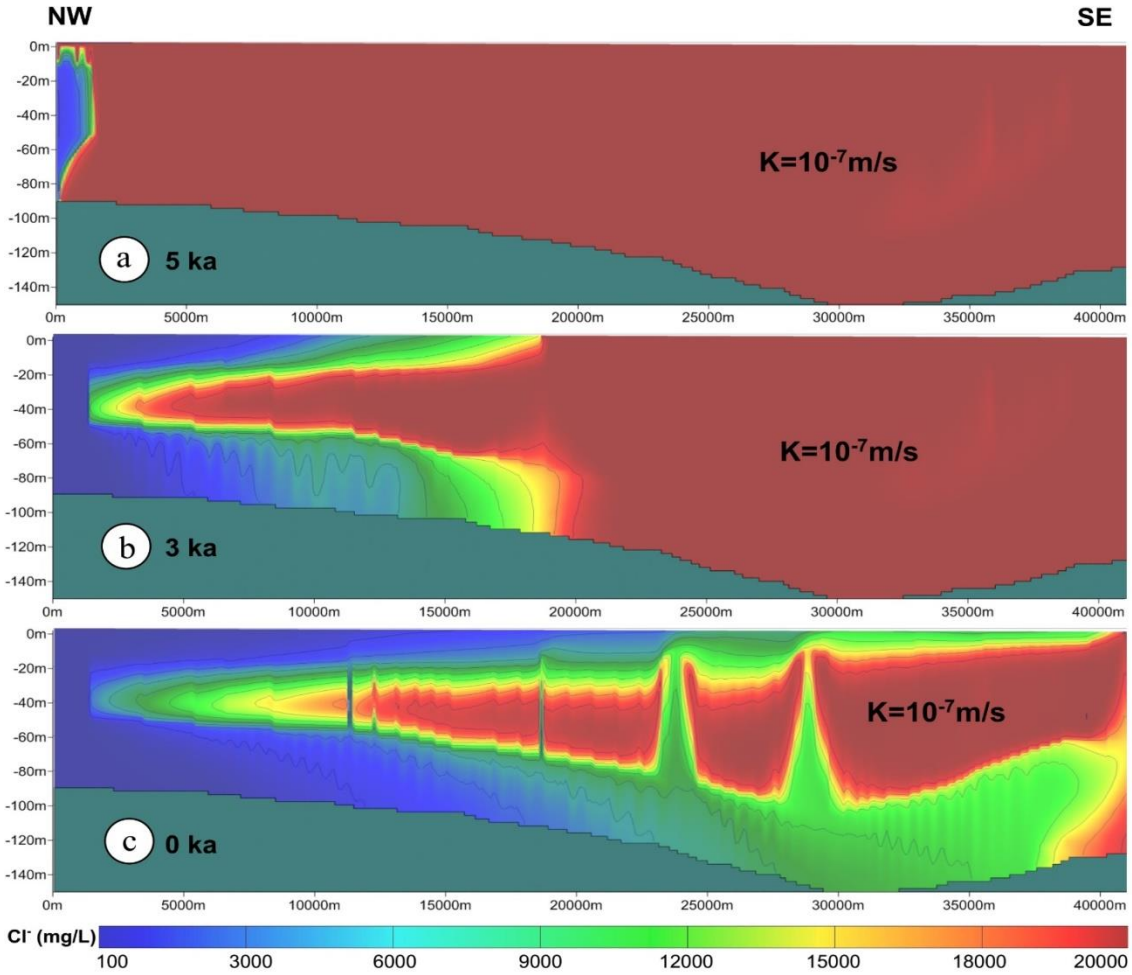

Figure 12. SEAWAT simulation results with hydraulic conductivity of the aquitard clay of 10^{-7} m/s. Initial concentration of chloride in the model domain is 20 g/L, ad results show concentrations after 5,000, 7,000 and 10,000 years of saltwater fluxing

5. Discussions

Some of the findings in this study regarding freshwater recharge and salinization processes in the Nam Dinh province seem to reveal general aspects regarding the occurrence of paleo-saltwater in the delta areas. In contrast, other elucidates processes that are of significance for managing the saltwater problem in the Nam Dinh province.

During pristine conditions in the Nam Dinh province, artesian conditions were observed in the Pleistocene aquifer before groundwater abstraction. The historical hydraulic head data and field observation also suggest an upward hydraulic gradient. This could point to an upward groundwater flow. The observed distribution of trapped pore water in the aquitard and the results of the

numerical groundwater modeling show that the transport of solute out of the aquitard layer is controlled mainly by diffusion. One explanation for this absence of an advective flow through the aquitard could be the presence of "threshold gradients" below which little or no flow occurs (Neuzil 1986). Olsen (1985) shows that a lack of advective flow can be explained by osmotic forces without inferring to non-Darcian flow conditions. Wooding et al. (1997) studied near-surface saline pond environments, with low permeable, salty clay overlying a permeable, fresh groundwater zone, and showed that below a threshold permeability of 10^{-14} m^2 (equivalent to the hydraulic conductivity of approximately 1×10^{-7} m/s) a near-surface salty the boundary layer was stable, and density induced convection did not occur. In these studies of near-surface sediments, an evaporative flux was present in the clay layer, diminishing the downward transport of solutes with the water. Using the Rayleigh number (Ra) as a criterion, Groen et al. (2000) argue that convective density flow occurs in a stratified system with saline groundwater overlying fresh groundwater. This occurs when this number exceeds a critical Rayleigh number value close to 40. The Rayleigh number is given by equation 2:

$$R_a = \frac{(\Delta\rho) g k H}{\nu D_e} \qquad (2)$$

Where $\Delta\rho$ is the density difference between the salt and fresh water, g is the acceleration of gravity, k is the permeability of the sediment, H is the thickness of the sediment with saltwater, ν the dynamic viscosity of the water and D_e is the effective diffusion coefficient. The parameters in equation 2, which may vary most, are the difference in water density, sediment permeability, and thickness of the layer with salty water. Using a maximum water density difference of 20 kg/m^3 (80% of seawater) and a saltwater layer thickness of 50 m, the onset of a convection density flow should at this study site occur when k exceeds 4×10^{-16} m^2 (4×10^{-9} m/s), which is a hydraulic conductivity, a factor 10 higher than observed in this study for the silty clays (Table 4). However, the variability in apparent resistivity in the aquitard, as revealed by the TEM soundings (Fig. 10), indicates variations in leaching of the salt water, and this could reflect variations in the hydraulic conductivity of the aquitard, thereby affecting the transport mechanism, with density-driven transport occurring in high permeability layers. Results of the conceptual 2D numerical groundwater flow simulation conducted in this study confirm that stratification of the water column, with saline water overlying brackish of fresh groundwater, can remain stable over thousands of years in the delta systems, with the permeability of the sediments as one of the controlling parameters of solute transport by diffusion in low permeable sediments.

Based on our knowledge, the most thorough determination of the permeability and porosity in unconsolidated and consolidated marine sediments was done by Bryant et al. (1975), who used laboratory consolidation tests to examine the samples from the Gulf of Mexico. In that study, marine sediments were divided into four groups; Group 1, sediments containing more than 80% clay-sized material (< 2 μm); Group 2, containing sediments from 60 to 80 % clay-sized material; Group 3, silty clays with less than 60%, and Group 4, silts and clays that have a significant sand-size fraction present (> 5%). These results showed the hydraulic conductivity in these sediments ranged from 10-7 to 10-12 m/s, and samples buried a few tens of meters had hydraulic conductivities below 10-9m/s. The clay samples from Nam Dinh province are comparable to the clays in Group 3 of Bryant et al. (1975), with a porosity of 30 and 40% and hydraulic conductivity of app. 10-11 m/s. These observations of hydraulic properties in

unconsolidated marine clays could suggest that diffusion-controlled transport of seawater out of transgressive clays is a general phenomenon in coastal aquifer systems, as similar stratified profiles reported from other studies of Quaternary coastal multi-aquifer systems (e.g. Radhakrishna 2001; Manzano et al. 2008; Hiroshiroe ty al 2006: Akouvi et al. 2008; Han et al. 2011; Ikawa et al. 2014).

In the numerical simulations of the groundwater flow, it is assumed that salty water is present in both high and low permeability formations as an initial condition. This might, however, be an unrealistic assumption, as there is worldwide documentation that fresh groundwater has been flowing into shelf sediments during the Holocene transgression (Manheim et al. 1968; Meisler et al. 1984; Post et al. 2013). In our simulations, a change of this initial condition would lead to more fresh or brackish groundwater in the Pleistocene aquifer.

A specific finding of significance for the distribution of salty groundwater in the Pleistocene aquifer (Fig. 1), and the management of the groundwater resource in the Nam Dinh province, is the hydraulics of the Late Pleistocene clay layer (Fig. 2a and 2b). In contrast to the Holocene aquitard, this layer is freshwater bearing, which is likely explained by flushing the Pleistocene marine clay with fresh water during the low water stand in the Early Holocene. In places where the Pleistocene clay is underlying the Holocene salty aquitard (Fig. 9), the Pleistocene aquifer contains freshwater. The flux of the marine pore water out of the Holocene aquitard solemnly by diffusion will ideally develop symmetrical chloride concentrations profiles, with upward and downward gradients into sandy layers, as seen in borehole Q222 (Fig. 9), where the Holocene clay is directly overlying the Pleistocene aquifer. Asymmetrical salinity profiles are encountered in the boreholes Q109, Q110, and Q 223, where downward leaching by diffusion occurs into underlying Pleistocene freshwater clay (Fig. 9). This shows that the freshwater bearing Pleistocene clay is reducing the downward flow of salty pore water into the Pleistocene aquifer, and this is the reason for the heterogeneous distribution of salty groundwater in this aquifer (Fig. 1).

There is a strong argument for a local hydraulic contact between the more profound and upper aquifer in the Nam Dinh province. Therefore, recharge to the deeper aquifers must only occur from the elevated mountain areas west of the region (Fig. 1). Before groundwater abstraction, groundwater flowed offshore through the high permeable Pleistocene layers. After groundwater pumping was initiated, a downward hydraulic gradient has been built up for approximately 25 years, reaching~ 160 ‰ in the central part of the cone of depression. At the same time, groundwater flow directions have been changed in the Pleistocene aquifer, with a flow controlled by the location of the recharge area and the location of the major groundwater abstraction points (Fig. 6).

With the observed decline in the water table in the Pleistocene aquifer, the present water abstraction rate may not be sustainable. A coastal saltwater intrusion may be generated with a further decline of groundwater level. The only monitoring borehole located between the abstraction point (Q109) and the sea is Q110 (Fig. 1), and this was drilled to a depth of approximately 50 m above the top of the Neogene layers. This borehole is therefore not deep enough to monitor if a saltwater intrusion has occurred in the Neogene layer. Freshwater resources might be present in the Pleistocene aquifer offshore stored in the Pleistocene deposits, but these will eventually be mined, and saltwater will then move into the aquifer. The dynamics of this system can only be studied with a three-dimensional variable-density groundwater flow model, and more work,

including offshore data, is thus necessary to explain this question.

6. Conclusions

From the investigations conducted on the salinization processes in the coastal aquifers in the Nam Dinh Province, it can be concluded that:

(1) The groundwater composition in the shallow aquifer is affected by leakage of saline river water into the aquifer at a distance up to 35 km from the coastline, and TDS values in the aquifer up to 6 g/L, have been observed. The hydraulics in the shallow aquifer is largely controlled by the water stage in the irrigation canals, into which water is transported in the dry season to irrigate the paddy field after the rice has been planted.

(2) The deep Pleistocene aquifer seems only to be recharged from the mountains west of the Nam Dinh province. During pristine conditions, freshwater flowed towards the sea in the deep aquifer and further offshore below the sea bottom.

(3) A Holocene transgressive marine clay separates the shallow and the deeper aquifers, and hydraulic and water stable isotope values suggest a limited hydraulic connection between the shallow and deep aquifers.

(4) The salinity distribution in the marine clay has been mapped using transient electromagnetic soundings and geophysical borehole logging.

(5) The numerical modeling results using the code SEAWAT show the distribution of pore water salinities resembling the mapped concentrations when aquitard hydraulic conductivities are below 10-8 m/s.

(6) In the present pumping controlled flow regime, dissolved solutes are transported by advection and diffusion from the confining Holocene layer into the Pleistocene aquifer.

(7) Saltwater intrusion from the sea into the Pleistocene aquifer might be generated in the future, but more studies are needed to confirm.

(8) As some uncertainties pointed out above, the paleo-climatic conditions related to paleo-groundwater recharge and the distribution of coastal paleo-seawater concentrations associated with the initial conditions of paleo-pore water in the sediments still need to be clarified in these upcoming studies

Acknowledgments

This work has been supported by the Danish Development Research Council (DANIDA) as part of a research capacity building project ‘‘Water Resources Research in Vietnam’’. We want to express our gratitude to Ingerlise Nørgård and Holger Lindgreen, both from GEUS, for conducting textural and X-ray analyses of the sediments. Christina Rosenberg Lynge and Pernille Stockmarr from GEUS did the water chemistry work in the laboratory, and they are thanked for this.

References

Akouvi A., Dray M., Violette S., de Marsily G., Zuppi G.M., 2008. The sedimentary coastal basin of Togo: example of a multilayered aquifer still influenced by a paleo-seawater intrusion. Hydrogeology, Jour., 16, 419-436.

Auken E., Nebel L., Sørensen K., Breiner M., Pellerin L., Christensen N.B., 2002. EMMA a geophysical training and education tool for electromagnetic modeling and analysis. Journal of Environmental and Engineering Geophysics, 7, 57-68.

Auken E., Christiansen A.V., Jacobsen B.H., Foged N., Sørensen K.I., 2005. Piecewise 1D Laterally Constrained Inversion of resistivity data: Geophysical Prospecting, 53, 497-506.

Bryant W.R., Hottman W., Trabant P., 1975. Permeability of Unconsolidated and Consolidated Marine Sediments, Gulf of Mexico. Marine Geotechnology, 1(1), 1-14.

Clark I., Fritz P., 1997. Environmental Isotopes in Hydrogeology, Lewis Publ., 328p.

Coplen T.B., Hanshaw B.B., 1973. Ultrafiltration by a compacted clay membrane - I. Oxygen and

hydrogen isotopic fractionation. Geochim. et Cosmochim. Acta, 87, 2205-2810.

Dansgaard W., 1964. Stable isotopes in precipitation. Tellus, 16, 436-468.

Edmunds W.M., 2001. Paleowater in European coastal aquifers -the goals and main conclusions of the PALAEAUX project. In: Edmunds WM and Milne CJ (eds). Paleowaters in Coastal Europe: evolution of groundwater since the late Pleistocene. Geol. Soc. Special Publ., 189, 1-16.

Fitterman D.V., Stewart M.T., 1986. Transient electromagnetic sounding for groundwater. Geophysics, 51, 995-1005.

Funabiki S., Nguyen V.Q., Viet P.H., Dinh H.T., 2007. Holocene delta plain development in the Song Hong (Red River) delta, Vietnam. J. Asian Earth Sci., 30, 518-529.

Groen J., Velstra J., Meesters A.G.C.A., 2000. Salinazation process in paleowaters in coastal sediments of Suriname: evidence from δ^{37} Cl analysis and diffusion modelling. Jour. Hydrology, 234, 1-20.

Guo W., Langevin C.D., 2002. User´s guide to SEAWAT: a computer program for simulation of three-dimensional variable-density ground-water flow. US Geol. Surv. Open-File Rep., 1-34.

IAEA, 2014. http://www-naweb.iaea.org/NAALIHL/docs/tech_info/ Precipitation%20 Sampling 97.pdf. The homepage was accessed July 8th, 2014.

Han D., Kohfahl C., Song X., Xio G., Yang J., 2011. Geotechnical and isotopic evidence for paleo-seawater intrusion into the south coast aquifer of Laizhou Bay, China. Applied Geochemistry, 26, 863-883.

Hanebuth T., Stattegger K., Bojanowski K., 2009. Termination of the Last Glacial Maximum sea level lowstand: Sundra-Shelf data revised. Global Planetary Change, 66, 76-84.

Hiroshiro Y., Jinno K., Berndtsson R., 2006. Hydrochemical properties of a salinity-affected coastal aquifer in western Japan. Hydrological Processes, 20, 1425-1435.

Hoang V.H., Lassen R., Tran V.L., Vu H.A., Pham Q.N., Larsen F., 2011. Mapping of fresh water and saline groundwater in a coastal aquifer in the Nam Dinh Province (Vietnam) by electrical and electromagnetic soundings. APOAMM, The First Asia-Pacific Coastal Aquifer Management Meeting: Mapping for Synergy in the Twenty-first Century, Bangkok, 9-11, December 2009.

Hoang V.H., Larsen F., Nguyen V.L., Dang D.N., Tran T.L., Pham Q.N., 2018. Salt Groundwater Intrusion in the Pleistocene Aquifer in the Southern Part of the Red River Delta, Vietnam. VNU Journal of Science: Earth and Environmental Sciences, 34(1), 11-22.

Hori K., Tanabe S., Saito Y., Haruvama S., Nguyen V., Kitamura A., 2004. Delta initiation and Holocene sea level change: example from the Song Hong (Red River) delta, Vietnam. Sedimentary Geology, 164, 237-249.

Ikawa R., Machida I., Koshigi M., Nishizaki S., Mariu A., 2014. Coastal aquifer system in late Pleistocene to Holocene deposits at Horonobe in Hokkaido, Japan. Hydrogeology Journal, 22, 987-1002.

Kolker A.S., Cable J.E., Johannesson K.H., Allison M.A., Inniss L.V., 2013. Pathways and processes associated with transport of groundwater in deltaic systems. Journal of Hydrology, 498, 319-334.

Langevin C.D., Guo W., 2006. MODFLOW/M3DMS-based simulation of variable-density ground-water flow and transport. Ground Water, 44, 339-351.

Larsen F., Pham N.Q., Dang N.D., Postma D., Jessen S., Pham V.H., Nguyen T.B., Trieu H.D., Tran L.T., Nguyen H., Chambon J., Nguyen H.V., Ha D.H., Hue N.T., Duc M.T., Refsgaard J.C., 2008. Controlling geological and hydrogeological processes in an arsenic contaminated aquifer on the Red River flood plain, Vietnam. Appl. Geochem., 23(11), 3099-3115.

Larsen F., Tran V.L., Hoang V.H., Tran T.L., Christiansen A.V., Pham Q.N., 2017. Groundwater salinity influenced by Holocene seawater trapped in incised valleys in the Red River delta plain. Nature Geoscience. Doi: 10.1038/ngeo2938.

Manzano M., Custodio E., Loosli H., Cabrera M.C., Riera X., Custodo J., 2001. Palaeowater in coastal aquifers of Spain. In Edmunds W. M., Milne C.J., 2001 Palaeowaters in Coastal Europe: evolution of groundwater since the Late Pleistocene. Geol. Soc., London. The Geo. Soc. of London, 189, 107-138.

MCDonald M.G., Harbaugh A.W., 1988. A modular three-dimensional finite-difference ground-water flow model, Tech. of Water-Resources Inv. 06-A1, USGS, 576p.

Manheim F.T., Horn M.K., 1968. Composition of deeper subsurface waters along the Atlantic continental margin. Southeast Geol., 9, 215-236.

Meisler H., Leahy P.P., Knobler L., 1984. Effect of Eustatic Sea level Changes on Saltwater-Freshwater Relations in the Northern Atlantic Coastal Plain. U.S. Geo. Survey Water Supply, pp. 2255.

Mills T., Hoekstra P., Blohm M., Evans L., 1988. Time-domain electromagnetic soundings for mapping sea-water intrusion in Monterey County, California. Groundwater, 26, 771-782.

Neilson-Welch L., Smith L., 2001. Saline water intrusion adjacent to the Fraser Riber, Richmond, British Columbia. Canada Geotech. Journal, 38, 67-82.

Neuzil C.E., 1986. Groundwater Flow in Low-Permeability Environments. Water Res. Res., 22(8), 1163-1195.

Nguyen V.D., 2009. Study on Hydrogeological conditions and current exploration of groundwater in a coastal zone of Nam Dinh - Northern Division for water Resources planning and Investigation.

Nguyen T.H., 2005. Groundwater chemistry and its behaviour in Quaternary sediments and possibility for water supply in Northern Plain, Vietnam. PhD dissertation report. Hanoi University of Mining and Geology, 159p.

Nguyen A.D., Savenije H.H.G., Pham D.N., Tang D.T., 2008. Using salt intrusion measurements to determine the freshwater discharge distribution over the branches of a multi-channel estuary: The Mekong Delta case. Estuarine. Coastal and Shelf Science, 77, 433-445.

Olsen H.W., 1985. Osmosis: A cause of apparent deviations from Darcy´s law. Can. Geotech. Journal, 22(2), 238-241.

Pham Q.N., 2000. Groundwater reserves in Red River delta plain and its sustainable development. PhD dissertation report. Hanoi University of Mining and Geology, 144p.

Pham Q.S., 2004. Study of development of Red River - That Binh River estuaries on the basis of Remote Sensing's Information and GIS for rational exploitation of use of territory. PhD thesis on Protection. Rational use and Generation of Natural resources, in Vietnamese. National University, 155p.

Post V.E.A., Groen J., Kooi H., Person M., Ge S., Edmunds W.M., 2013. Offshore fresh groundwater reserves as a global phenomenon Nature, 504, 71-78.

Postma D., Larsen F., Nguyen T.M.H., Mai T.D., Pham H.V., Pham Q.N., Jessen S., 2007. Arsenic in groundwater of the Red River floodplain, Vietnam: controlling geochemical processes and reactive transport modelling. Geochim. Cosmochim. Acta, 71, 5054-5071.

Radhakrishna I., 2001. Saline fresh water interface structure in Mahanadi delta region, Orissa, India Environmental Geology, 40(3), 369-380.

Reeburgh W.S., 1967. An improved interstitial water sampler. Limnol. Oceanogr., 12, 163-165.

Rozanski K., Araguás-Araguás L., Gonfiantini R., 1993. Isotope patterns in modern global precipitation. In Continental Isotope Indicators of Climate, American Geophysical Union Monograph.

Stewart M.T., 1982. Evaluation of Electromagnetic Methods for Rapid Mapping of Saltwater Interfaces in Coastal Aquifers. Ground Water, 20, 583-545.

Stookey L.L., 1970. Ferrozine - a new spectrophotometric reagent for iron. Anal. Che., 42, 779-781.

Tanabe S., Saito Y., Quang L.V., Hanebuth T.J.J., Quang L.N., Kitamura A., 2006. Holocene Evolution of the Song Hong (Red River) delta system, northern Vietnam. Sediment. Geol., 187, 29-61.

Tavenas F., Jean P., Leblond P., Leroueil S., 1983. The permeability of natural soft clays. Part II: Permeability characteristics, Can. Geotech. Journal, 20, 645-660.

Tran N., Ngo Q.T., Do T.V.T., Nguyen D.M., Nguyen V.V., 1991. Quaternary sedimentation of the principal deltas of Vietnam. J. Southeast Asian Earth Sci., 6, 103-110.

Tran L.T., Larsen F., Pham Q.N., Christiansen A.V., Tran N., Vu H.V., Tran L.V., Hoang H.V., Hins K.,

2012. Origin and extent of fresh groundwater, salty paleowaters and recent saltwater intrusions in the Red River flood plain aquifers, Vietnam. Hydrogeology Journal, 20, 1295-1313.

Vu T.C., 1996. Salinity Intrusion in the Red River delta. Seminar on Env. and Development in Vietnam, December 6-7, 1996. (Available via http://coombs.anu.edu.au/~vern/ env_dev/papers/pap08.html. Accessed July 8th, 2014).

Waelbroeck C., Labeyrie L., Michael E., Duplessey J., McManus J., Lambeck K., Balbon E., Labracherie M., 2002. Sea level and deep water temperature changes derived from benthic foraminifera isotopic records. Quaternary Science Reviews, 21, 295-305.

Wagner F., Dang T.T., Hoang D.P., Lindenmaier F., 2011. Assessment of Groundwater Resources in Nam Dinh Province. Improving groundwater protection in Vietnam - Final Technical Report Part A, National Center for Water Resources Planning and Investigation (CWRPI) & Federal Institute for Geosciences and Natural Resources. Hannover, 149p. http://www.bgr.bund.de/EN/Themen/Wasser/Projekte/laufend/TZ/Vietnam/techn_report_phase1_partA_en.pdf?__blob=publicationFile&v=9.

Wooding R.A., Tyler S.W., White I., 1997. Convection in groundwater below an evaporating salt lake: 1. Onset of instability. Water Res. Research, 33(6), 1199-1217.

Zapico M.M., Vales S., Cherry J.C., 1987. A wine-line piston core barrel for sampling cohesionless sand and gravel below the water-table. Ground Water Monitoring and Remediation, 7(3), 74-82.

Zheng C., Wang P.P., 1998. MT3DMS, A modular three-dimensional multispecies transport model for simulation of advection, dispersion and chemical reactions of contaminations in groundwater systems: Vicksburg, Miss. Waterways Experiment Station. U.S. Army Corps of Engineers.

Zhang W., Feng H., Zheng J., Hoitink A.J.F., van der Vegt M., Zhu Y., Cai H., 2013. Numerical Simulation and Analysis of Saltwater Intrusion Lengths in the Pearl River Delta. China. Journal of Coastal Res., 29(2), 372-382.